Influence of proton and neutron deformed shells on the asymmetric fission of thorium isotopes

A. Chatillon,[1,2,*] J. Taïeb,[1,2] A. Heinz,[3] H. Alvarez-Pol,[4] L. Audouin,[5] Y. Ayyad,[4,†] G. Bélier,[1,2] J. Benlliure,[4] G. Boutoux,[1] M. Caamaño,[4] E. Casarejos,[6] D. Cortina-Gil,[4] A. Ebran,[1,2] F. Farget,[7] B. Fernández-Domínguez,[4] T. Gorbinet,[1] L. Grente,[1] H. T. Johansson,[3] B. Jurado,[8] A. Kelić-Heil,[9] N. Kurz,[9] B. Laurent,[1,2] J.-F. Martin,[1] C. Nociforo,[9] C. Paradela,[4,‡] E. Pellereau,[1] S. Pietri,[9] A. Prochazka,[9] J. L. Rodríguez-Sánchez,[4,§] D. Rossi,[9,‖] H. Simon,[9] L. Tassan-Got,[5] J. Vargas,[4,¶] B. Voss,[9] and H. Weick[9]

[1]*CEA, DAM, DIF, F-91297 Arpajon, France*
[2]*Université Paris-Saclay, CEA, Laboratoire Matière en Conditions Extrêmes, 91680 Bruyères-le-Châtel, France*
[3]*Chalmers University of Technology, 41296 Gothenburg, Sweden*
[4]*IGFAE, Universidade de Santiago de Compostela, E-15782, Santiago de Compostela, Spain*
[5]*Université Paris-Saclay, CNRS, IJCLab, 91405 Orsay, France*
[6]*CINTECX - Universidade de Vigo, E-36310 Vigo, Spain*
[7]*CNRS, GANIL, Bd H. Becquerel, 14076 Caen, France*
[8]*CNRS, LP2I Bordeaux, F-33175 Gradignan, France*
[9]*GSI-Helmholtzzentrum für Schwerionenforschung GmbH, D-64291 Darmstadt, Germany*

(Received 12 June 2020; revised 13 June 2022; accepted 8 August 2022; published 31 August 2022)

Mean values of the number of protons and neutrons of the primary fission fragments at scission are determined for the asymmetric fission of 16 fissioning isotopes, from ^{219}Ac up to ^{238}Np. Our results confirm that the main asymmetric fission mode around the heavier uranium isotopes is indeed characterized by an average atomic number around $\langle Z_H \rangle = 54$ in the heavy fission fragments. However, they also unambiguously show a stabilization effect in the light fission fragments around $\langle N_L \rangle = 52$–54 in the neutron-deficient thorium and actinium isotopes. This is a clear signature that these deformed proton and neutron shell closures around 54 play a major role in the nuclear fission process. The evolution along the thorium chain shows that the neutron shell appears to be dominant in the asymmetric fission of the lighter thorium isotopes, in contrast to the heavier thorium isotopes for which the stabilization originates from the proton shell.

DOI: 10.1103/PhysRevC.106.024618

I. INTRODUCTION

Fission at low excitation energy is strongly governed by nuclear structure; the mass and charge distributions of the fission fragments are prominently influenced by shell and pairing effects. The macroscopic liquid drop model [1] describes the fission path along a single-humped fission barrier, and thus predicts symmetric fission. On the contrary, including microscopic effects [2], with a double-humped fission barrier description characterized by an outer barrier with a lower height for octupole deformation [3,4], is the only way to explain the deformed ground state of the fissioning nucleus, the fission isomers, but also the asymmetric fission observed in the fission-fragment mass distributions [5–7]. The early fission experiments were performed in direct kinematics, for which a beam of neutrons, protons, γ rays, or light-charged particles impinges on a stable or long-lived fissile target. Due to the limited availability of targets, mainly heavy actinides around the near stable region, from thorium up to californium, were studied [8]. Asymmetric fission was found to be characterized by heavy fission fragments distributed around a mean mass $\langle A_H \rangle \approx 138$–$140$, while the mean mass of the light fission fragments increases with the mass of the fissioning nucleus [8,9]. This was one of the first signatures of the influence of nuclear shell structure on the fission fragments, more specifically on the heavy one. Moreover, these fission-fragment mass distributions were also measured in coincidence with the total kinetic energy (TKE) of the fragments [7,10–13] and the prompt-neutron multiplicity [7]. From correlating such observables, an interpretation of fission in this region was proposed, based on its decomposition into three fission modes [14–16], two asymmetric and one symmetric. These modes, governed by the shell structure of the fission fragments, correspond to specific paths along the fission valleys of the potential energy surface (PES), each with their own barrier and scission configurations. Thus, the first asymmetric mode, the so-called standard I (ST1) mode, is influenced

*audrey.chatillon@cea.fr
†Present address: National Superconducting Cyclotron Laboratory, Michigan State University, East Lansing, MI 48824-1321, USA.
‡Present address: EC-JRC, Institute for Reference Materials and Measurements, Retieseweg 111, B-2440 Geel, Belgium.
§Present address: GSI-Helmholtzzentrum für Schwerionenforschung GmbH, D-64291 Darmstadt, Germany.
‖Present address: Technische Universität Darmstadt, Fachbereich Physik, Institut für Kernphysik Schlossgartenstrasse 9, 64289 Darmstadt, Germany.
¶Present address: Universidad Santo Tomás, Tunja, Colombia.

by the doubly magic shell closure around ^{132}Sn, leading to an almost spherical heavy fragment and a compact scission configuration. The second and dominating asymmetric mode, referred as the standard II (ST2) mode, is characterized by a heavy fragment stabilized at $\langle A_H \rangle \approx 138$–$140$, as previously mentioned. The origin of this mode will be discussed subsequently. Finally, a symmetric path leading to two highly deformed fission fragments defines the superlong (SL) mode. The latter becomes dominant as the excitation energy increases. These modes are difficult to study in classic direct kinematics experiments. Indeed experimental constraints, especially fluctuations of the ionic charge states in energy-loss measurements of the fission fragments, prevent the determination of the nuclear charge of the fission fragments in the heavy group. The atomic number identification is then limited, usually to the light group [17].

Experimental studies took a huge step forward with the advent of fission experiments performed in inverse kinematics. Thanks to the kinematic boost, such experiments provide data with an improved charge resolution for both light and heavy fission fragments. At the GSI facility, experiments based on inverse kinematics using radioactive actinide beams at relativistic energies were performed in the 1990s [18]. Fission of a broad range of radioactive nuclei, encompassing neutron-deficient isotopes from ^{205}At up to ^{234}U, was electromagnetically induced and the nuclear charge yields were precisely measured. This breakthrough allowed us to study the influence of proton shells on fission and a new insight into the nature of the ST2 asymmetric fission mode was obtained [19]. Theoretical interpretations of this mode from the 1970s were based on neutron shells, either with the presence of the deformed neutron shell in the heavy fragments around $N_H \approx 88$ [20], or, due to the strong coupling of the fissioning system at the saddle point to the neutron orbitals [$40\Lambda\Omega$] and [$51\Lambda\Omega$] [21]. On the contrary, the data showed that the heavy fission fragments are stabilized around an average atomic number $\langle Z_H \rangle \approx 54$ [18], with $\langle Z_{H,ST2} \rangle \approx 54$–$56$ [19]. More recent experiments also performed in inverse kinematics but measuring the isotopic yields confirmed that asymmetric scission is characterized by an average atomic number located around $\langle Z_H \rangle \approx 54$ [22–24]. This value is very slowly decreasing when the fissioning nucleus becomes more neutron rich, indicating an increase of the influence of the ST1 mode when the N/Z ratio becomes closer to that of ^{132}Sn. But still, the ST1 mode remains the less important asymmetric mode, and the origin of the ST2 asymmetric mode was still an open question. Recently, a theoretical study has related it to the presence of octupole-deformed shells in the ^{144}Ba region [25]. Given that the evolution of a fissioning nucleus towards a scission configuration results in extreme deformations, the ST2 mode, governed by deformed shell gaps, is favored compared to the ST1 mode, which is related to the doubly magic spherical shell closures at $Z = 50$ and $N = 82$.

Similarly, fission of ^{180}Hg is an excellent textbook case to probe the role of the spherical shell gaps in fission. One could expect that the influence of spherical shells located at $Z = 40$ and $N = 50$ would cause nuclei in the ^{180}Hg region to fission symmetrically. However, asymmetric fission was observed [26] and confirmed by several experiments based on fusion-fission, which extend this island of asymmetric fission from sub-lead to bismuth neutron-deficient fissioning isotopes [27–30]. In Ref. [26] and based on the calculated five-dimensional (5D) fission potential-energy landscape [31,32], this asymmetric fission is interpreted as totally unrelated to any fission-fragment shells. Such description considers this asymmetric fission as a new mode, since it strongly differs from the asymmetric fission in actinides, stabilized by the influence of proton shells in the heavy fission fragments. On the contrary, the previously mentioned theoretical studies [25] have been extended to this ^{180}Hg region and give a different interpretation. Asymmetric fission is related to the octupole-deformed shell gaps at $N_H = 52$ and 56 in the heavy fission fragments [33]. In Refs. [28,29] the measured position of the centroids of the mass distributions are consistent with the presence of deformed proton and neutron shell gaps located at $Z_L = 32$–38, $Z_H \approx 45$, and $N_L = 56$. In contrast, in Ref. [30], the complete isotopic distribution of the fission fragments measured for the fission of ^{178}Hg indicates the dominant role of the proton shells only around $Z_L = 36$. Therefore, the role of neutron-deformed shells in the fission process is still an open question.

In this paper, we present an experimental study of the influence of proton and neutron shells on the fission of thorium isotopes from ^{222}Th to ^{230}Th. The experiment was performed at GSI by the R3B/SOFIA (Reactions with Relativistic Radioactive Beams/Studies On FIssion with Aladin) collaboration. Fission of thorium isotopes was induced by Coulomb excitation, with a mean excitation energy for the (γ,f) reaction around 13–14 MeV [34]. At such excitation energies, the shell effects still have a dominant role in the fission process, confirmed by the comparison of ^{233}U(n_{th},f) [35,36] with ^{234}U(γ,f) [23], or of ^{229}Th(n_{th},f) [37] with ^{230}Th(γ,f) [34]. Therefore, this experiment is a suitable tool to study the underlying shell effects in low-energy fission of nuclei, which cannot be studied by direct kinematics experiments. Thanks to data obtained within the same experiment, results obtained for these thorium isotopes are compared to those from three neighboring actinium isotopes, ^{219,223,227}Ac, but also to those from the well-known heavier actinide region, ^{228,229,231,232}Pa, ^{234,235,238}U, and ^{238}Np isotopes. Such a comparison highlights that nuclear fission in these two regions, neutron-deficient light actinides on one side, and heavier actinides on the other side, is stabilized by different shells.

II. MEAN VALUES OF THE FISSION YIELDS

The setup and the analysis are discussed in detail in Refs. [22,23,34]. On an event-by-event basis, radioactive beams and fission fragments are identified in terms of their nuclear charge and mass in coincidence. Thus, fission yields and total prompt-neutron multiplicity are extracted for a wide range of fissioning systems, from actinium ($Z_{CN} = 89$) up to neptunium ($Z_{CN} = 93$).

A. Fitting procedure

Elemental, isotonic, and isobaric yields measured with the R3B/SOFIA setup and published in Refs. [22–23] are fitted with a function composed of three Gaussian functions to

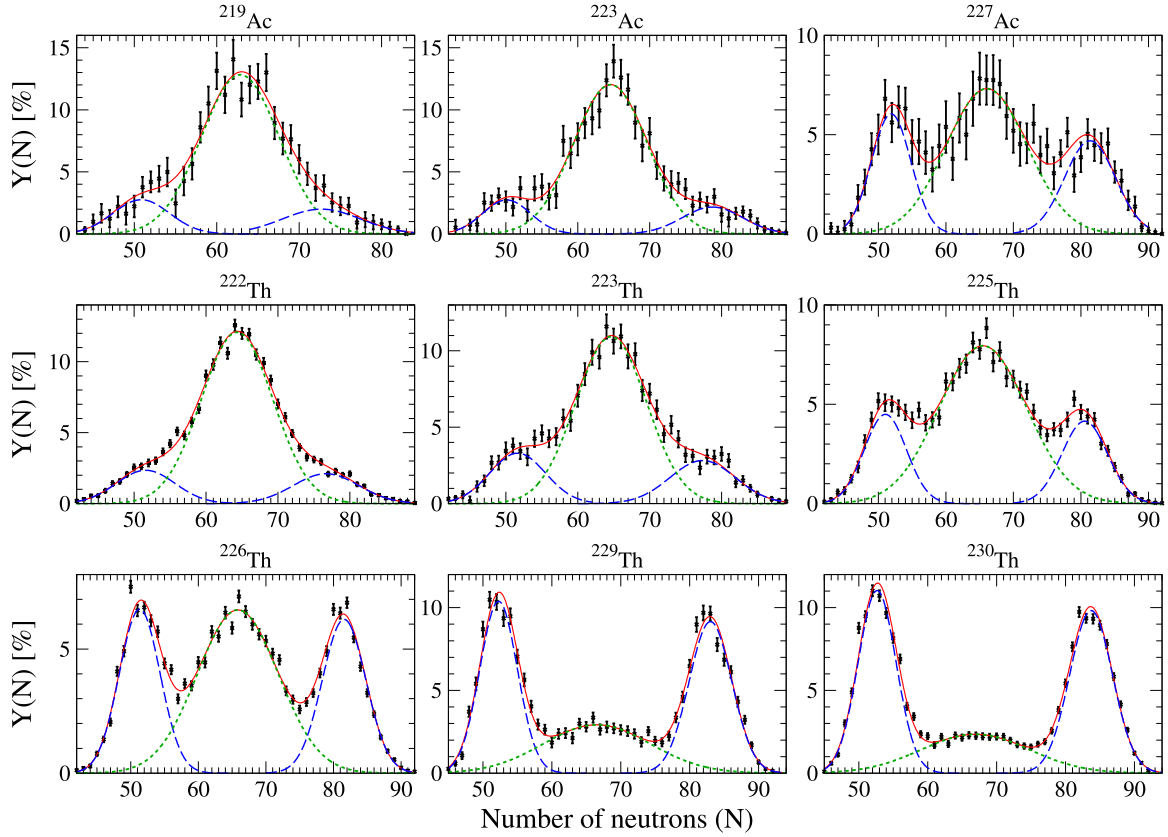

FIG. 1. Isotonic yields after prompt-neutron emission for each of the actinium and thorium isotopes fitted by a 3-Gaussian function. The data measured from the R3B/SOFIA experiments are in black. The error bars represent the statistical uncertainties. The total fit (full red lines) is decomposed into one symmetric (dotted green lines) and two asymmetric (dashed blue lines) components.

extract the mean position of the light, symmetric and heavy peaks. We extended the analysis presented in Ref. [34] in order to study a larger range of the fissioning nuclides. It was finally possible to obtain the mean values of the isotonic and isobaric yields for the ^{219,223,227}Ac, ^{223}Th, and ^{229}Pa fissioning nuclei (see Appendix A). In case of the isotonic and isobaric yields, the width of the heavy component is different than that of the lighter one. Therefore, an additional constraint is added in the multifit to ensure that the light and heavy components have the same integral yield. The fitting procedure is illustrated in Fig. 1 for the measured isotonic yields of the actinium and thorium isotopes. The 3-Gaussian fits are represented by the full red lines, the asymmetric components by the dashed blue lines and the symmetric one by the dotted green lines. Mean values obtained for the asymmetric components from the fits of the elemental, isotonic and isobaric yields can be found in Table I. The case of ^{221}Th was discarded, since the asymmetric component is too weak to obtain mean values with reasonable error bars.

To crosscheck the analysis procedure, the ratio between the symmetric and the asymmetric components is presented in Fig. 2 for the thorium fissioning nuclei. The latter is obtained from the multifit of the elemental (full red squares), isotonic (open black triangles), or isobaric (open blue circles) yields. All results are consistent. Moreover, the centroid positions of the light and heavy components of the fission fragment mass distribution, directly obtained from the fit of the isobaric yields, are compared to those inferred from the sum of the mean values of the atomic and neutron numbers, respectively, obtained from the fits of the elemental and isotonic yields. Figure 3 shows this comparison for each fissioning nuclide measured in this experiment. Therefore, Figs, 2 and 3 confirm that the centroid positions of the light, symmetric, and heavy peaks of the elemental, isotonic, and isobaric distributions are reliable.

Finally, a first tendency appears for the thorium fissioning nuclei: The average mass number of the heavy fission fragments decreases with decreasing mass number of the fissioning nucleus, whereas the average mass of the light fission fragments is stable around $\langle A_L \rangle \approx 88$. As previously mentioned in Sec. I, this behavior is in contrast to what has been observed in the asymmetric fission of heavier actinides where the mass of the heavy fission fragments is centered around $\langle A_H \rangle \approx 138$–$140$, while the mean mass of the light fission fragments increases with the mass of the fissioning nucleus [8,9]. This observation is the starting point of this paper: Do we see a stabilization effect in the light fission fragments? And what is the origin of such a stable mass in the light group? Since it is now well known that the atomic number of the heavy fragment group is centered around $Z_H = 54$ (see Ref. [18] and Sec. II B), for thorium isotopes, the atomic number of the light fission fragments can only be centered

TABLE I. Centroid positions of the light and heavy peaks of the fission yields measured after neutron evaporation.

Nuclide	$\langle Z_L \rangle$	$\langle N_L \rangle$	$\langle A_L \rangle$	$\langle Z_H \rangle$	$\langle N_H \rangle$	$\langle A_H \rangle$
^{219}Ac	36.1 ± 0.6	50.8 ± 1.1	87.7 ± 2.1	52.9 ± 0.6	72.7 ± 1.3	125.3 ± 2.4
^{220}Ac	36.1 ± 0.8	–	–	52.9 ± 0.8	–	–
^{223}Ac	35.2 ± 0.7	50.1 ± 1.0	85.7 ± 1.3	53.8 ± 0.7	78.7 ± 1.2	132.2 ± 1.6
^{227}Ac	35.9 ± 0.4	51.9 ± 0.4	87.7 ± 0.6	53.1 ± 0.4	81.3 ± 0.6	134.3 ± 0.8
^{222}Th	36.5 ± 0.5	51.4 ± 1.0	87.8 ± 1.7	53.5 ± 0.5	76.9 ± 1.4	130.6 ± 2.0
^{223}Th	36.2 ± 0.5	51.6 ± 0.8	87.8 ± 1.1	53.8 ± 0.5	77.4 ± 1.1	131.2 ± 1.3
^{225}Th	36.1 ± 0.2	51.0 ± 0.5	87.1 ± 0.7	53.9 ± 0.2	80.5 ± 0.6	134.4 ± 0.8
^{226}Th	35.7 ± 0.1	51.3 ± 0.2	87.0 ± 0.3	54.3 ± 0.1	81.6 ± 0.2	136.0 ± 0.3
^{229}Th	35.9 ± 0.1	52.3 ± 0.2	88.2 ± 0.3	54.1 ± 0.1	83.0 ± 0.2	137.0 ± 0.3
^{230}Th	35.9 ± 0.1	52.7 ± 0.1	88.5 ± 0.2	54.1 ± 0.1	83.7 ± 0.1	137.8 ± 0.2
^{228}Pa	36.8 ± 0.1	52.5 ± 0.2	89.2 ± 0.3	54.2 ± 0.1	80.9 ± 0.2	135.1 ± 0.3
^{229}Pa	36.7 ± 0.1	53.0 ± 0.2	89.6 ± 0.3	54.3 ± 0.1	81.8 ± 0.2	136.2 ± 0.3
^{231}Pa	36.9 ± 0.1	53.6 ± 0.2	90.7 ± 0.2	54.1 ± 0.1	83.0 ± 0.3	137.2 ± 0.3
^{232}Pa	36.9 ± 0.1	54.3 ± 0.1	91.3 ± 0.2	54.1 ± 0.1	83.5 ± 0.2	137.3 ± 0.3
^{234}U	38.1 ± 0.1	55.7 ± 0.1	93.8 ± 0.1	53.9 ± 0.1	83.0 ± 0.1	136.9 ± 0.1
^{235}U	38.2 ± 0.1	56.1 ± 0.1	94.3 ± 0.1	53.8 ± 0.1	83.3 ± 0.1	137.0 ± 0.1
^{238}U	38.6 ± 0.1	58.3 ± 0.1	96.6 ± 0.1	53.4 ± 0.1	84.2 ± 0.1	137.8 ± 0.1
^{237}Np	39.2 ± 0.1	57.6 ± 0.1	96.5 ± 0.2	53.8 ± 0.1	83.1 ± 0.2	137.1 ± 0.2
^{238}Np	39.3 ± 0.1	58.1 ± 0.1	97.5 ± 0.2	53.7 ± 0.1	83.3 ± 0.2	137.2 ± 0.2

around $Z_L = 36$. The fluctuation of the mass is thus directly linked to the fluctuations of the neutron number. Therefore, a stable mass in the light group might be consistent with a stabilization due to the influence of a neutron shell.

The role of proton and neutron shell structure is studied in detail in the following, to gain insight into the origin of the constant mass of the light fission fragments in fissioning thorium isotopes.

B. Mean values of the atomic number

The role of the proton shells of the fission fragments during the fission process, can be probed directly by fitting the elemental yields with a function composed of three Gaussian functions (see Sec. II A). The mean values of the asymmetric components obtained from the fit of the elemental yields, are represented in Fig. 4 and compared to the measurements of Refs. [18,22–24]. For all fissioning isotopes investigated in Ref. [18], the average atomic number of the heavy fission

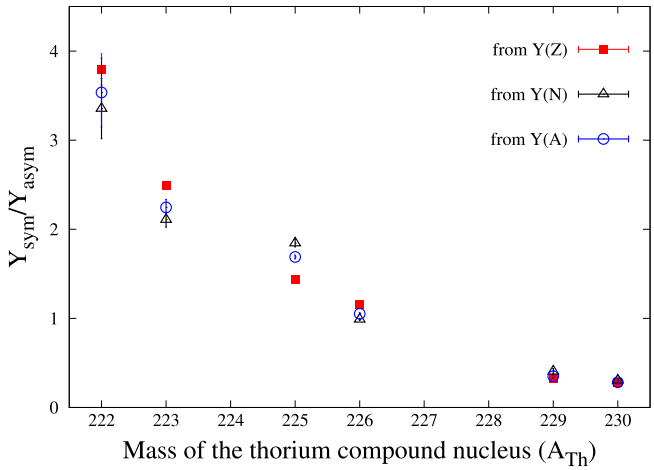

FIG. 2. Ratio between the symmetric and asymmetric components for the thorium nuclides, inferred from the multifit of the elemental (full red squares), isotonic (open black triangles) and isobaric (open blue circles) yields.

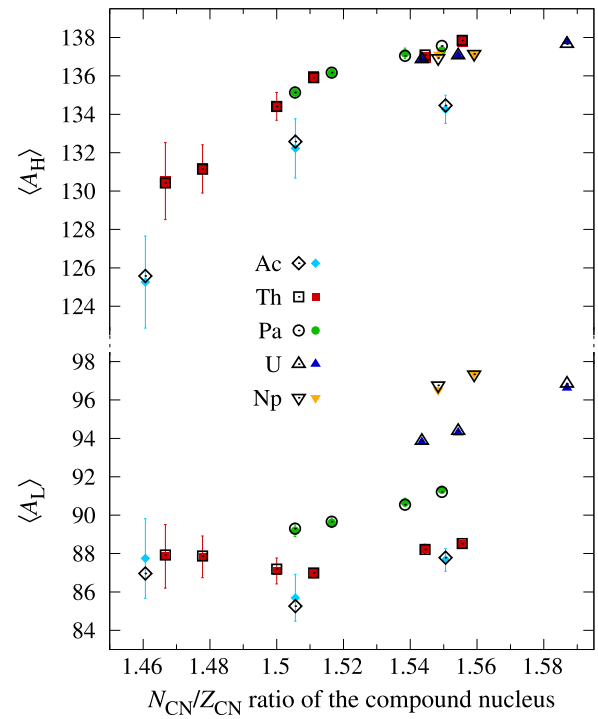

FIG. 3. The average value of the mass of the light and heavy fission fragments from the measured isobaric yields (colored full symbols) are compared to the sum (open black symbols) of the mean nuclear charge and mean number of neutrons.

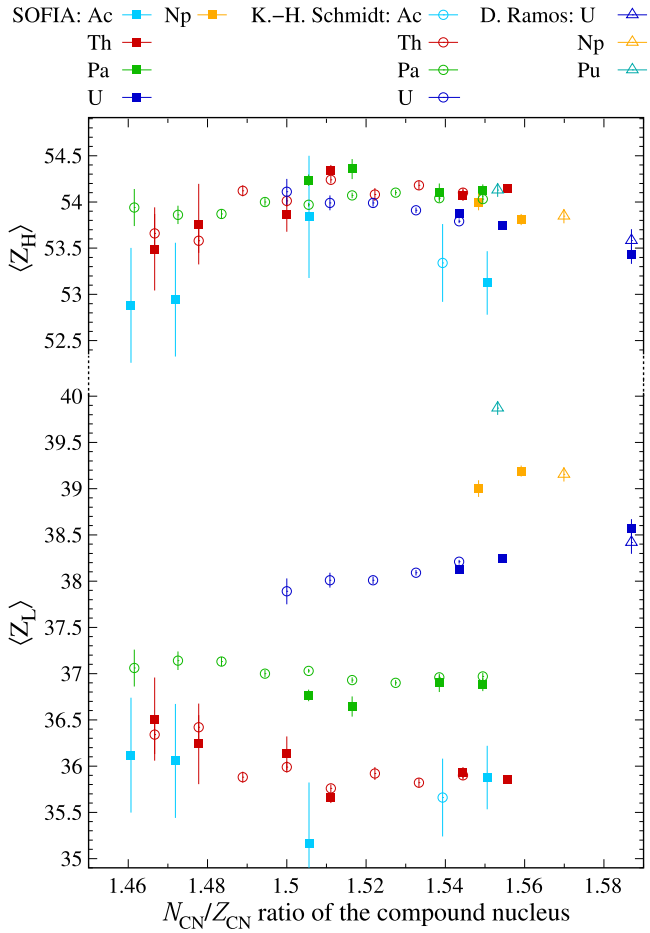

FIG. 4. The average value of the atomic number of the light and heavy fission fragments measured at R3B/SOFIA (full squares) are compared with data from Refs. [18,19] (open circles) and [24] (open triangles).

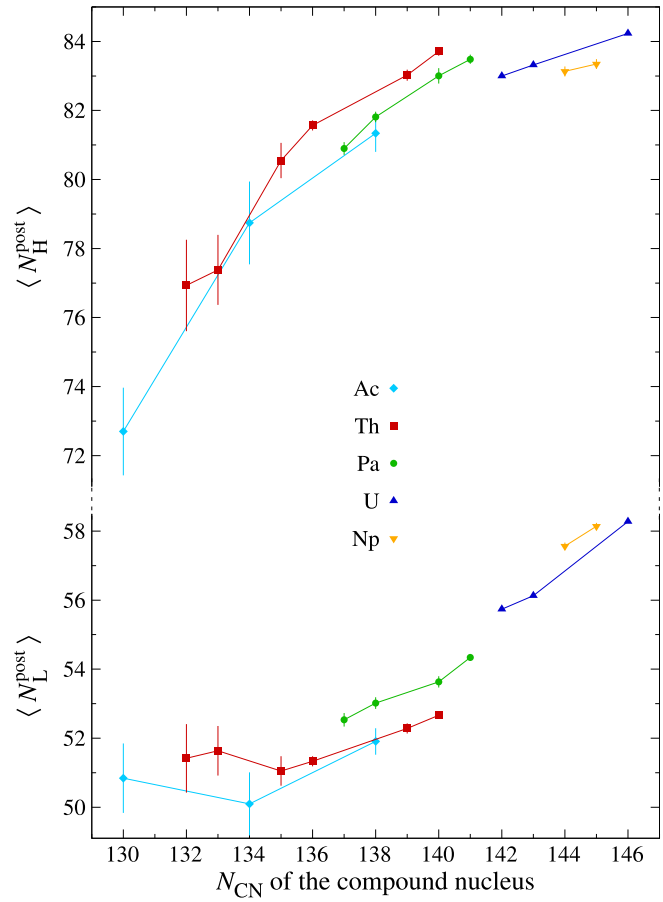

FIG. 5. Centroid positions of the light and heavy peaks of the isotonic yields measured after the prompt-neutron evaporation phase.

fragment, $\langle Z_H \rangle$, is also observed to be close to 54, whereas the average atomic number of the light fission fragment compensates the difference with respect to the number of protons of the compound nucleus, $\langle Z_L \rangle \approx Z_{CN}$–54. This suggests that the deformed proton shell closure located around $Z = 54$ plays a major role in the population of the fission fragments in asymmetric fission, especially for fissioning nuclei with a N_{CN}/Z_{CN} up to 1.55. Above 1.55, the $\langle Z_H \rangle$ mean value decreases. As mentioned in the introduction, this is understood as the increased influence of the ST1 mode governed by the doubly-magic ^{132}Sn. Finally, the influence of the deformed shell at $Z_H = 54$ is also weakened for thorium isotopes for which $N_{CN}/Z_{CN} \leqslant 1.49$. This feature could not be identified in Ref. [18]. Indeed, due to the smaller statistics the mean value of the heavy component was fixed to $\langle Z_H \rangle = 54$ in the 3-Gaussian fit for the $^{217–221}$Th isotopes in that work. Finally, the actinium isotopes have a different behavior and can be considered as transitional nuclides for which the effect of $\langle Z_H \rangle = 54$ starts to vanish. Indeed, except for ^{223}Ac ($N_{CN}/Z_{CN} = 1.506$), the value of the mean atomic number for the heavy group is below $\langle Z_H \rangle = 54$, whereas for the light group, it is close to $\langle Z_L \rangle = 36$ as for the thorium isotopes.

C. Mean values of the neutron number

As far as the isotonic yields are concerned, the mean values of the neutron number of the light and heavy fission fragments, $\langle N_{L,H}^{post} \rangle$, are shown in Fig. 5, for the actinium, thorium, protactinium, uranium, and neptunium isotopes. These values are given as a function of the N_{CN} ratio of the compound nucleus. For the uranium isotopic chain, from ^{234}U to ^{238}U, $\langle N_L^{post} \rangle$ increases by more neutrons (2.5 neutrons) than $\langle N_H^{post} \rangle$ (1.2 neutrons). Both neptunium isotopes follow also the same trend as the uranium ones. This is expected and also explained in Ref. [18] and more recently in Ref. [23]. The influence of the proton shells around $Z_H = 54$ stabilizes the heavy fragment while the light fragment compensates for the number of nucleons. Moreover, the influence of the $N_H = 82$ neutron shell also plays a role since it acts as a trap during the evaporation phase: The large neutron binding energy hinders prompt-neutron evaporation. However, as shown in Fig. 5, this statement is fully valid only for uranium and neptunium fissioning nuclei. For protactinium, thorium, and actinium, all measured below $Z_{CN}/N_{CN} = 1.54$ and $N_{CN} = 136–138$, the trend is reversed. Over the four mass units range in the $^{228–232}$Pa isotopic chain, the increase of $\langle N_L^{post} \rangle$ by 1.8 neutrons, is smaller than that of $\langle N_H^{post} \rangle$ by 2.6 neutrons. The evolution of $\langle N_{L,H}^{post} \rangle$ over the mass range of the $^{222–230}$Th

TABLE II. Average total prompt-neutron multiplicity and statistical uncertainties, for the full ($\langle\nu^{\rm tot}\rangle$) and asymmetric ($\langle\nu^{\rm tot}_{\rm asym}\rangle$) ranges of the fission fragments. When the systematic uncertainties are not negligible, they are indicated between brackets. GEF is used to infer the part of the prompt-neutron multiplicity emitted by the compound nucleus ($\nu_{\rm CN}$), thus obtaining the total prompt-neutron multiplicity emitted by the fission fragments only ($\langle\nu^{\rm tot}_{\rm FF,asym}\rangle$). Finally, from the hypothesis of Eq. (1), the number of prompt neutron emitted by the light and heavy fragments are obtained ($\langle\nu_{\rm L,H}\rangle$).

Nuclide	$\langle\nu^{\rm tot}\rangle$	$Z_{\rm L}$ and $Z_{\rm H}$ ranges	$\langle\nu^{\rm tot}_{\rm asym}\rangle$	$\nu_{\rm CN}$ [%]	$\langle\nu^{\rm tot}_{\rm FF,asym}\rangle$	$\langle\nu_{\rm L}\rangle$, $\langle\nu_{\rm H}\rangle$
^{219}Ac	4.7 ± 0.1	[33,37] [52,56]	5.8 ± 0.3 (±0.1)	4.8	5.5 ± 0.3 (±0.1)	2.3, 3.2 ± 0.3 (±0.5)
^{223}Ac	4.7 ± 0.1	[33,37] [52,56]	4.4 ± 0.3	11.1	3.9 ± 0.3	1.5, 2.4 ± 0.3 (±0.4)
^{227}Ac	5.5 ± 0.1	[33,38] [51,56]	5.3 ± 0.2	13.2	4.6 ± 0.2	1.8, 2.8 ± 0.2 (±0.4)
^{222}Th	3.57 ± 0.03	[33,37] [53,57]	3.5 ± 0.1	5.6	3.3 ± 0.1	1.3, 2.0 ± 0.1 (±0.4)
^{223}Th	3.86 ± 0.05	[33,37] [53,57]	4.0 ± 0.2 (±0.1)	8.6	3.7 ± 0.2 (±0.1)	1.5, 2.2 ± 0.2 (±0.5)
^{225}Th	4.08 ± 0.04	[33,38] [52,57]	3.8 ± 0.1 (±0.1)	10.8	3.4 ± 0.1 (±0.1)	1.3, 2.1 ± 0.1 (±0.5)
^{226}Th	3.81 ± 0.03	[33,38] [52,57]	3.4 ± 0.1 (±0.2)	10.2	3.0 ± 0.1 (±0.2)	1.2, 1.8 ± 0.1 (±0.5)
^{229}Th	4.26 ± 0.04	[33,38] [52,57]	3.8 ± 0.1 (±0.1)	17.2	3.1 ± 0.1 (±0.1)	1.2, 1.9 ± 0.1 (±0.5)
^{230}Th	4.22 ± 0.03	[33,38] [52,57]	3.8 ± 0.1 (±0.1)	15.5	3.2 ± 0.1 (±0.1)	1.3, 1.9 ± 0.1 (±0.5)
^{228}Pa	3.85 ± 0.03	[33,38] [53,58]	3.7 ± 0.1 (±0.1)	7.2	3.4 ± 0.1 (±0.1)	1.4, 2.0 ± 0.1 (±0.5)
^{229}Pa	3.49 ± 0.04	[33,38] [53,58]	3.4 ± 0.1 (±0.1)	8.1	3.1 ± 0.1 (±0.1)	1.2, 1.9 ± 0.1 (±0.5)
^{231}Pa	3.41 ± 0.05	[33,39] [52,58]	3.3 ± 0.1	11.4	2.9 ± 0.1	1.1, 1.7 ± 0.1 (±0.4)
^{232}Pa	3.74 ± 0.04	[33,39] [52,58]	3.5 ± 0.1	14.4	3.0 ± 0.1	1.2, 1.8 ± 0.1 (±0.4)
^{234}U	3.56 ± 0.01	[33,39] [53,59]	3.4 ± 0.1	5.4	3.2 ± 0.1	1.3, 1.9 ± 0.1 (±0.4)
^{235}U	3.75 ± 0.01	[33,39] [53,59]	3.6 ± 0.1	7.8	3.3 ± 0.1	1.3, 2.0 ± 0.1 (±0.4)
^{238}Np	4.04 ± 0.03	[33,40] [53,60]	3.9 ± 0.1	5.8	3.7 ± 0.1	1.5, 2.2 ± 0.1 (±0.4)

fissioning nuclei is even more striking. Indeed, $\langle N^{\rm post}_{\rm H}\rangle$ increases by 6.8 neutrons, while it turns out that the light component is stable around $\langle N^{\rm post}_{\rm L}\rangle \approx 51$–$52$. This is particularly true for the neutron-deficient side, where the influence of $Z_{\rm H} = 54$ begins to be weaker, as mentioned in Sec. II B and shown in Fig. 4. For actinium nuclides, the same behavior, a smaller increase of $\langle N^{\rm post}_{\rm L}\rangle$ than $\langle N^{\rm post}_{\rm H}\rangle$, is also observed.

This constant value in number of neutrons seems to indicate that neutron shells also play a role during the nuclear fission process. In our data, this is observed in the light fission fragment group for fission of neutron-deficient nuclides around the thorium nuclei. However, to decouple the nuclear structure effects, which play a role during fission from the ones that act as a trap during the evaporation phase, the number of neutrons of the primary fragments, prior to the prompt-neutron emission, needs to be inferred, following the method described in Ref. [23] and summarized in Sec. III A. Results on the number of neutrons of the primary fission fragments are finally given in Sec. III B.

III. INFLUENCE OF NEUTRON SHELLS: METHOD AND RESULTS

A. Fission as an adiabatic process using a Fermi gas hypothesis

Our measurement takes place after the prompt-neutron evaporation phase. Event-by-event, the R3B/SOFIA setup provides, with good accuracy, the total prompt-neutron multiplicity for each pair of fragment partners, $\langle\nu_{\rm tot}\rangle(Z_{\rm FF_1}, Z_{\rm FF_2})$ [23,38]. Within the same experiment, 16 fissioning nuclides have been studied: six thorium isotopes ^{222,223,225,226,229,230}Th covering a large range in N/Z, which can be compared to three actinium isotopes ^{219,223,227}Ac and seven heavier and well-known actinides ^{228,229,231,232}Pa, ^{234,235}U, and ^{238}Np. All results obtained during this experiment, concerning $\langle\nu_{\rm tot}\rangle$ in coincidence with the elemental yields, are given in Appendix B. This correlation measurement between $\langle\nu_{\rm tot}\rangle$ and fission yields is the starting point of the method detailed in Ref. [23].

Such a method can be applied to the 16 fissioning nuclides, studied with sufficient statistics to measure $\langle\nu^{\rm tot}\rangle(Z_{\rm FF_1}, Z_{\rm FF_2})$. Indeed, this total neutron multiplicity per atomic number is averaged over the nuclear charge ranges covering the light and heavy fission fragments, in order to extract $\langle\nu^{\rm tot}_{\rm asym}\rangle$, the total prompt-neutron multiplicity emitted during asymmetric fission only. The part of the prompt-neutron multiplicity emitted by the compound nucleus is calculated using the general description of fission observable model (GEF-2021-V1.1 [39]), in order to obtain $\langle\nu_{\rm tot,FF}\rangle$ the total prompt-neutron multiplicity emitted by both fission partners only. By assuming a certain sharing of this neutron multiplicity between the light and heavy fragments, one can obtain $\langle\nu\rangle(Z_{\rm FF_{L,H}})$, the prompt-neutron multiplicity emitted by the light and heavy groups, respectively. One method to distribute $\langle\nu\rangle(Z_{\rm FF_{L,H}})$ between both fission fragments, considers that the full excitation energy of each fission fragment translates into prompt-neutron emission at scission, and that the sharing of the excitation energy between both fragments follows an adiabatic process in a Fermi gas. As a consequence, the ratio of the masses of the primary fission fragments is equal to the ratio of the excitation energies:

$$\frac{\langle A^{\rm pre}_{\rm L}\rangle}{\langle A^{\rm pre}_{\rm H}\rangle} = \frac{\langle E^{*}_{\rm L}\rangle}{\langle E^{*}_{\rm H}\rangle} \approx \frac{\langle\nu_{\rm L}\rangle}{\langle\nu_{\rm H}\rangle}, \tag{1}$$

$$\langle\nu_{\rm L,H}\rangle = \langle\nu_{\rm tot,FF}\rangle(Z_{\rm L}, Z_{\rm H})\frac{\langle A_{\rm L,H}\rangle}{\langle A_{\rm L}\rangle + \langle A_{\rm H}\rangle}. \tag{2}$$

All numerical values are given in Table II. The uncertainty of this method arises from the fact that the excitation energy dis-

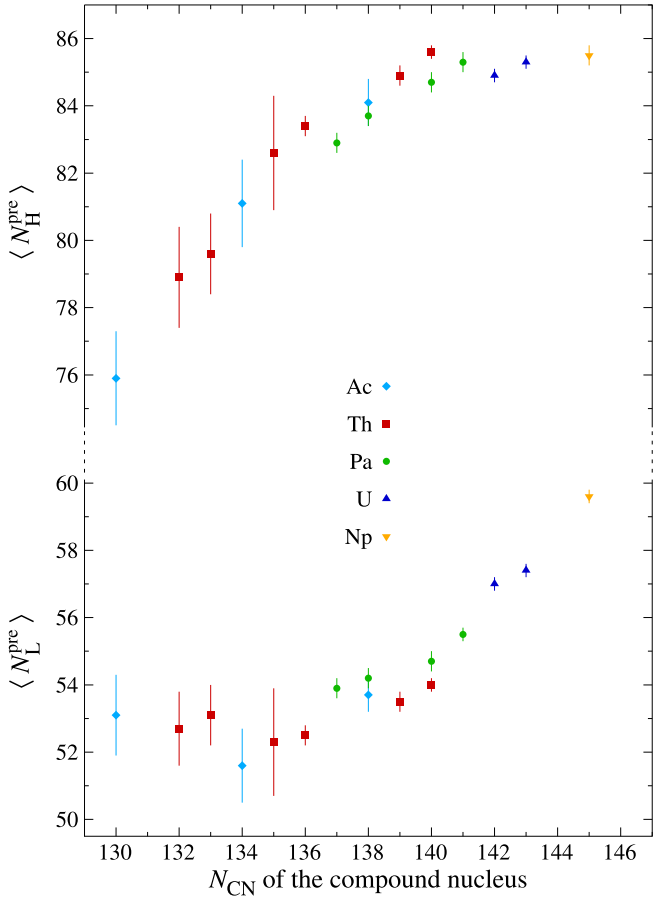

FIG. 6. Centroid positions of the light and heavy primary fission fragments, obtained prior to the prompt-neutron evaporation phase.

sipated by γ emission is neglected together with that gained after scission from the relaxation of the deformation energy. However, and it is quite important to insist on this point, this uncertainty is partly compensated since $\langle \nu_{tot} \rangle$ is measured for each (Z_L, Z_H) configuration with the R3B/SOFIA setup. Therefore $\langle \nu_{tot} \rangle$ already contains the information of the sum impact of deformation and γ emission. The sharing thus proposed in Eqs. (1) and (2) only neglects the differential impact between the light and heavy fragments, of deformation and γ emission. In Ref. [23], this approach has been compared to another sharing only based on experimental data obtained for the ^{234,235}U and ^{238}Np fissioning nuclei. The remaining bias, from the above-mentioned differential impact of deformation and γ emission, cannot be compensated but is evaluated to be lower than 0.4 neutrons for Coulomb-induced fission where the total prompt-neutron multiplicity is low.

B. Stabilization around $N_L = 52 - 54$

The average number of neutrons of the light and heavy primary fission fragments, are obtained from:

$$\langle N^{pre} \rangle (Z_{FF_{L,H}}) = \langle N^{post} \rangle (Z_{FF_{L,H}}) + \langle \nu \rangle (Z_{FF_{L,H}}). \quad (3)$$

Figure 6 demonstrates the stabilization for thorium chain. The mean neutron number in the primary light fission fragment is found to be around $\langle N_L^{pre} \rangle \approx 52$–$54$ over the full range of

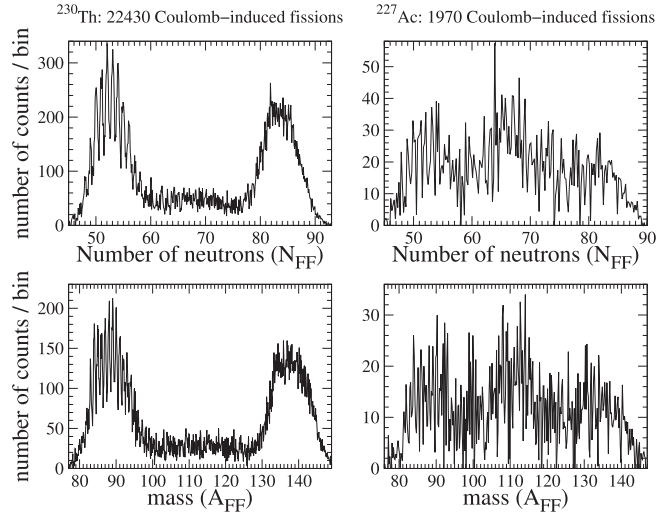

FIG. 7. For the FRS setting centered around the ^{230}Th isotope: comparison of the isotonic (top row) and isobaric (bottom row) distributions between the centered isotope and the less populated ^{227}Ac isotope.

the investigated thorium isotopes. The evolution of $\langle N_L^{pre} \rangle$ is flat for $^{222–226}$Th, and it slightly increases by one neutron for $^{226–230}$Th. The comparison with Fig. 4 shows interestingly an opposite trend. The mean proton number of the heavy fission fragments is stable around $\langle Z_H \rangle = 54$ for $^{225–230}$Th, and then it slightly decreases for $^{222–225}$Th. Both figures show that asymmetric fission along the thorium isotopic chain originates from a combination of the influence of two nuclear shells. Not only the proton number in the heavy fragments but also the neutron number in the light fragments, both around 54, play a major role in the asymmetric fission of the thorium nuclides. This result is a strong experimental evidence of the impact of the deformed proton and neutron shells around 54, on the nuclear fission process. Despite the larger uncertainties of the new results on Coulomb-induced fission of ^{219,223,227}Ac, the latter are in perfect agreement with the evolution observed along the thorium chain: it is the heavy fission fragment, which compensates the number of neutrons while the light fission fragment is stabilized around $\langle N_L^{pre} \rangle = 52$–$54$. Similarly, protactinium isotopes follow the same trend, but, since no sufficiently neutron-deficient isotopes were measured in this experiment, the asymptotic value is certainly not yet reached.

IV. CONCLUSION

Using electromagnetic-induced fission in inverse kinematics at relativistic energies, the R3B/SOFIA collaboration provides correlated data between fission yields (elemental, isotonic, and isobaric yields), and, the total prompt-neutron multiplicity. A particular effort to characterize fission along the thorium isotopes has been performed to observe the underlying influence of both proton and neutron shells. Since the reaction mechanism produces fissioning nuclei with an excitation energy around 13–14 MeV on average for thorium up to neptunium isotopes and around 16 MeV for actinium isotopes, the nuclear shell structure still has a dominant role and can be inferred from such data.

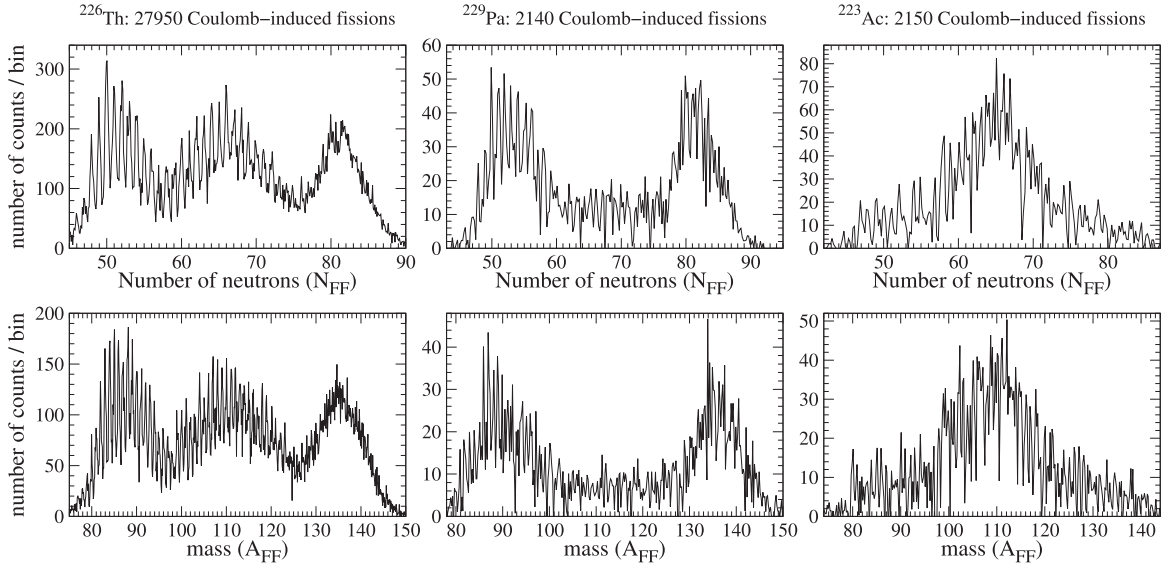

FIG. 8. For the FRS setting centered around the ^{226}Th isotope: comparison of the isotonic (top row) and isobaric (bottom row) distributions between the centered isotope and the less populated ^{229}Pa and ^{223}Ac isotopes.

In a first step, the influence of a deformed proton shell in the heavy fragments around $Z_H \approx 54$ was confirmed, from neptunium down to thorium isotopes, based on measured elemental yields. We also observed that the influence of $Z_H \approx 54$ weakens in the fission of thorium isotopes with $N_{CN}/Z_{CN} \leqslant 1.49$ and appears to vanish for actinium isotopes.

In a second step, the mean values of the isotonic distributions of primary fission-fragments were inferred. Unambiguously for the lighter thorium isotopes, but also with larger error bars for actinium isotopes, we observe that the light primary fission fragments in asymmetric fission are produced around $N_L^{pre} \approx 52$–54, indicating the influence of a deformed neutron shell in this region. This work is a first experimental observation of a neutron-shell stabilization around $N \approx$ 52–54 in the light fission fragments. It would be interesting to perform dedicated calculations and more experiments around this neutron-deficient thorium region to understand the reason why the asymmetric fission is not anymore stabilized by $Z_H = 54$ but rather by $N_L = 54$.

APPENDIX A: COULOMB-INDUCED FISSION OF ^{219,223,227}Ac, ^{223}Th, AND ^{229}Pa

During the experiments, three FRS settings were applied, centered around the ^{230,226,222}Th isotopes. Due to the weaker statistics for the ^{219,223,227}Ac, ^{223}Th, and ^{229}Pa isotopes, the latter were discarded in Ref. [34] to extract the isotonic and isotopic yields. However, the calibration parameters are the

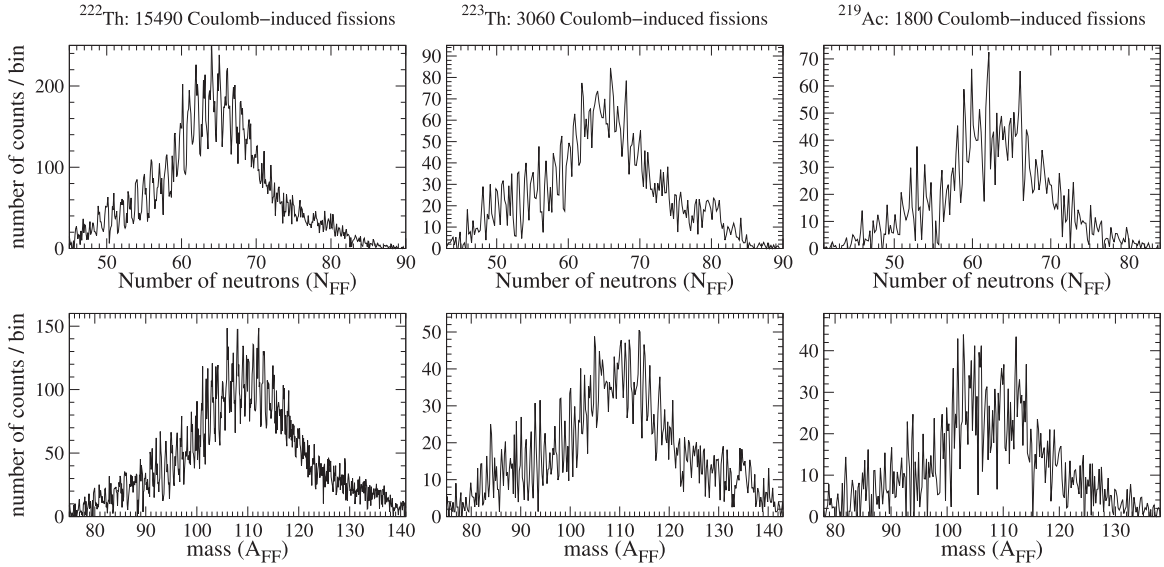

FIG. 9. For the FRS setting centered around the ^{222}Th isotope: comparison of the isotonic (top row) and isobaric (bottom row) distributions between the centered isotope and the less populated ^{223}Th and ^{219}Ac isotopes.

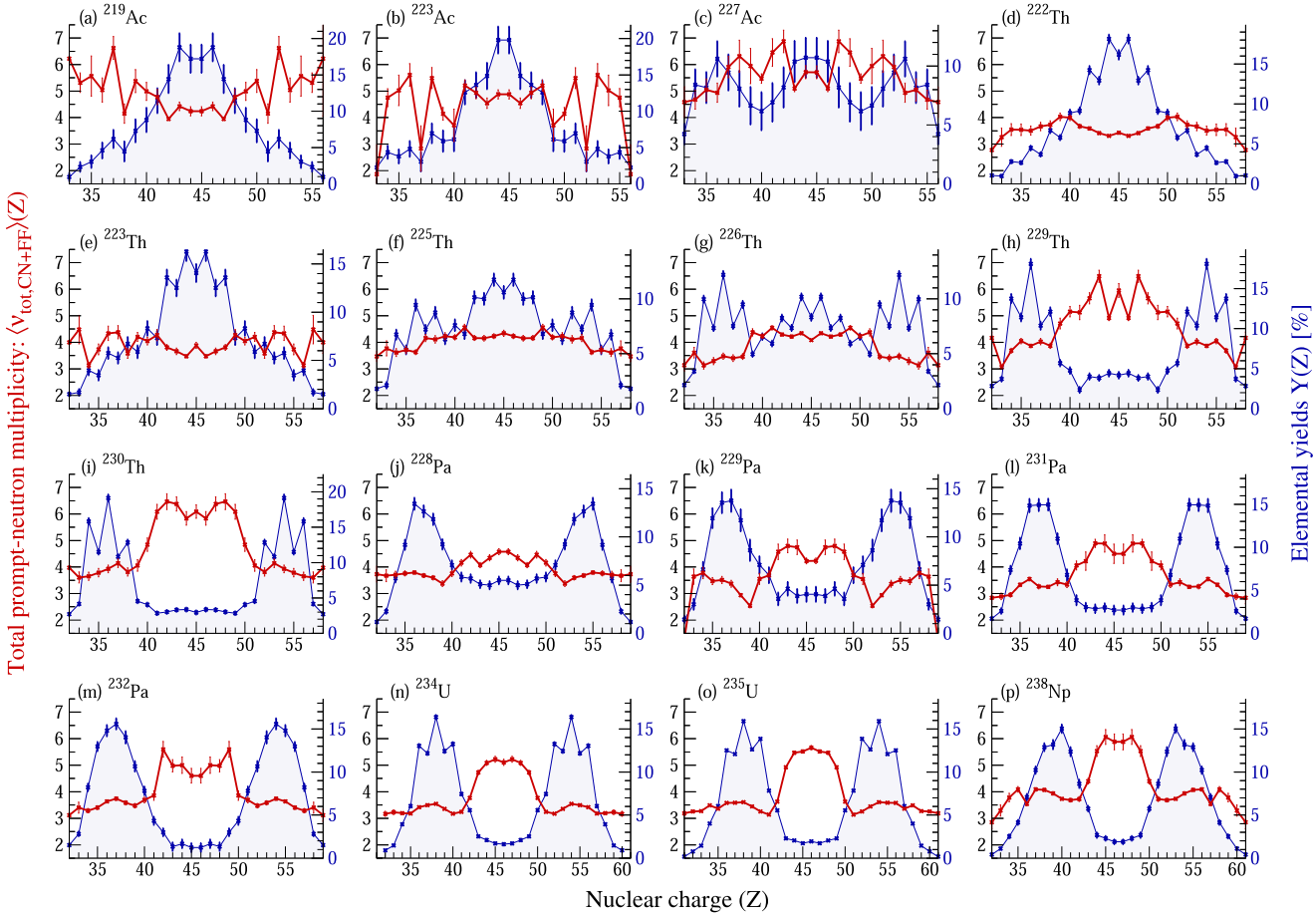

FIG. 10. For all nuclides measured in the experiment [23,38], elemental yields (right axis) are represented in blue and total prompt-neutron multiplicity (left axis) are represented in red.

same for each FRS setting, and are validated with the centered isotopes. Therefore, as shown in this section, it is still possible to obtain some reasonable values for the mean values of the isobaric and isotonic yields, with larger uncertainties. Figures 7–9 present the comparison of the isobaric and isotonic distributions measured in the Coulomb-induced fission of these less populated isotopes with the centered ones, for the FRS settings centered around ^{230}Th, ^{226}Th, and ^{222}Th, respectively.

APPENDIX B: MEASUREMENT OF THE TOTAL PROMPT-NEUTRON MULTIPLICITY

All results concerning $\langle\nu^{\mathrm{tot}}\rangle$ obtained during this first SOFIA experiment are plotted in dark red in Fig. 10, together with the elemental yields represented in blue. The total prompt-neutron multiplicity probes the evolution not only of the deformation at scission of the different symmetric and asymmetric configurations, but also of the average excitation energy of the different fissioning nuclei. Indeed a higher prompt-neutron multiplicity may indicate either a larger deformation of the primary fission fragments at scission, or, a higher excitation energy of the fissioning system. First, as detailed in Ref. [38], the neutron-deficient actinides mainly fission symmetrically and exhibit a dramatic decrease of the prompt-neutron multiplicity for these symmetric configurations. This is a clear signature that this fission mode is compact in contrast to the symmetric SL mode of heavier actinides and described in Sec. I. Second, the total prompt-neutron multiplicity is larger for actinium isotopes. This agrees very well with the evolution of the excitation energy of the fissioning systems, which is given in Refs. [22–24]. The excitation function of the (γ,tot) reaction is distributed up to 30 MeV with an average around 12 MeV for all nuclei. However, since the fission barrier is higher for actinium isotopes, the mean average excitation energy of the (γ,f) reaction is at least 3 MeV higher, inducing a higher prompt-neutron multiplicity for this element.

[1] N. Bohr and J. A. Wheeler, Phys. Rev. **56**, 426 (1939).
[2] V. M. Strutinsky, Nucl. Phys. A **95**, 420 (1967).
[3] P. Möller and S. G. Nilsson, Phys. Lett. B **31**, 283 (1970).
[4] H. C. Pauli, T. Ledergerber, and M. Brack, Phys. Lett. B **34**, 264 (1971).
[5] O. Hahn and F. Strassmann, Naturwissenschaften **27**, 11 (1939).

[6] W. E. Nervik, Phys. Rev. **119**, 1685 (1960).
[7] H. W. Schmitt, J. H. Neiler, and F. J. Walter, Phys. Rev. **141**, 1146 (1966).
[8] K. F. Flynn, E. P. Horwitz, C. A. A. Bloomquist, R. F. Barnes, R. K. Sjoblom, P. R. Fields, and L. E. Glendenin, Phys. Rev. C **5**, 1725 (1972).
[9] J. P. Unik, J. E. Gindler, L. E. Glendenin, K. F. Flynn, A. Gorski, and R. K. Sjoblom, in *Proc. Symp. Physics and Chemistry of Fission* (IAEA, Vienna, 1974), Vol. 2.
[10] M. Asghar, F. Caïtucoli, B. Leroux, M. Maurel, P. Perrin, and G. Barreau, Nucl. Phys. A **373**, 225 (1982).
[11] H. Thierens, E. Jacobs, P. D'hondt, A. De Clercq, M. Piessens, and D. De Frenne, Phys. Rev. C **29**, 498 (1984).
[12] C. Wagemans, E. Allaert, A. Deruytter, R. Barthélémy, and P. Schillebeeckx, Phys. Rev. C **30**, 218 (1984)
[13] C. Wagemans, P. Schillebeeckx, and A. Deruytter, Nucl. Phys. A **502**, 287 (1989)
[14] U. Brosa, Phys. Rev. C **38**, 1944 (1988).
[15] F.-J. Hambsch, H.-H. Knitter, and C. Budtz-Jørgensen, Nucl. Phys. A **491**, 56 (1989).
[16] U. Brosa, S. Grossmann, and A. Müller, Phys. Rep. **197**, 167 (1990).
[17] H.-G. Clerc, K.-H. Schmidt, H. Wohlfarth, W. Lang, H. Schrader, K. E. Pferdekämper, and R. Jungmann, Nucl. Instrum. Meth. **124**, 607 (1975).
[18] K.-H. Schmidt *et al.*, Nucl. Phys. A **665**, 221 (2000).
[19] C. Böckstiegel *et al.*, Nucl. Phys. A **802**, 12 (2008).
[20] B. D. Wilkins, E. P. Steinberg, and R. R. Chasman, Phys. Rev. C **14**, 1832 (1976).
[21] C. Gustafsson, P. Möller, and S. G. Nilsson, Phys. Lett. B **34**, 349 (1971).
[22] E. Pellereau *et al.*, Phys. Rev. C **95**, 054603 (2017).
[23] J.-F. Martin *et al.*, Phys. Rev. C **104**, 044602 (2021).
[24] D. Ramos *et al.*, Phys. Rev. C **97**, 054612 (2018).
[25] G. Scamps and C. Simenel, Nature (London) **564**, 382 (2018).
[26] A. N. Andreyev *et al.*, Phys. Rev. Lett. **105**, 252502 (2010).
[27] I. Tsekhanovich *et al.*, Phys. Lett. B **790**, 583 (2019).
[28] B. M. A. Swinton-Bland *et al.*, Phys. Rev. C **102**, 054611 (2020).
[29] E. Prasad *et al.*, Phys. Lett. B **811**, 135941 (2020).
[30] C. Schmitt *et al.*, Phys. Rev. Lett. **126**, 132502 (2021).
[31] P. Möller, D. G. Madland, A. J. Sierk, and A. Iwamoto, Nature (London) **409**, 785 (2001).
[32] P. Möller, A. J. Sierk, T. Ichikawa, A. Iwamoto, R. Bengtsson, H. Uhrenholt, and S. Aberg, Phys. Rev. C **79**, 064304 (2009).
[33] G. Scamps and C. Simenel, Phys. Rev. C **100**, 041602(R) (2019).
[34] A. Chatillon *et al.*, Phys. Rev. C **99**, 054628 (2019).
[35] U. Quade *et al.*, Nucl. Phys. A **487**, 1 (1988).
[36] F. Martin *et al.*, Nucl. Data Sheets **119**, 328 (2014).
[37] J. P. Bocquet, R. Brissot, H. R. Faust, M. Fowler, J. Wilhelmy, M. Asghar, and M. Djebara, Z. Phys. A: At. Nucl. **335**, 41 (1990).
[38] A. Chatillon *et al.*, Phys. Rev. Lett. **124**, 202502 (2020).
[39] K.-H. Schmidt, B. Jurado, C. Amouroux, and C. Schmitt, Nucl. Data Sheets **131**, 107 (2016).